Chapter 2
Exohedral Metallofullerenes

2.1 Monoatomic Doping

Fullerene-based materials have attracted considerable interest since the discovery of C_{60}. A promising area of research concerns metal–fullerene interactions and their application to advanced nano materials, with potential use in optical and switching devices, as photoconductors, and for hydrogen storage. Moreover, transition metal complexes of fullerenes show catalytic activity in homogeneous hydrogenation of acetylenic alcohols [1] and hydroformylation of alkenes [2]. In heterogeneous catalysis, exohedral metallofullerenes are found to promote hydrogenation of olefins and acetylenes [3, 4] as well as reduction of carbon monoxide to methane [5, 6].

The first exohedral metallofullerenes to be synthesized and isolated were η^2 complexes of $C_{60}Pt(PPh_3)_2$ and $C_{60}Pd(PPh_3)_2$ [7–9]. This work was later extended to monoatomic coordination by a whole range of metals including Ti, Nb, Re, Fe, Ru and Ni, and also multiple metal doping [4, 10–13].

Although geometry optimisation and calculation of electronic properties of metallofullerenes is time consuming because of the size of the system, the development of density functional theory (DFT) methods has made it possible to obtain accurate theoretical results for these systems. There are a limited number of theoretical studies published on exohedral transition metal complexes of fullerenes [14–16]. Most of the attention has been on the interaction of fullerenes with $M(PH_3)_2$ where M is a transition metal atom. The choice of metals was restricted to a single group in the periodical table, and to our knowledge there are no systematic studies of geometry and bonding in metal–fullerene complexes reported so far.

Except for one early report [17] on the bond dissociation energies for the naked nickel–fullerene complex, there is little information available about relative stabilities and dissociation energies of bare metal–fullerene complexes. Why does some metals form strong bonds to fullerenes, while the exohedral metallofullerene CoC_{60} has never been observed? The aim of our study is to shed light on this and related issues, by exploring which factors play important roles in metal–fullerene interactions and hence determine the bond strengths. To this end we study the interaction between

O. Loboda, *Quantum-Chemical Studies on Porphyrins, Fullerenes and Carbon Nanostructures*, Carbon Nanostructures, DOI: 10.1007/978-3-642-31845-0_2,

C_{60} and naked transition metal atoms of group 9 and 10, by means of DFT. Various possible bonding modes of C_{60} to metal atom are explored, including coordination with different hapticity. The M–C_{60} bonds are analyzed in terms of electron donation and back donation and repulsive polarization.

2.1.1 Method of Calculations

The geometries of metallofullerenes were optimized using density functional theory in terms of the OLYP functional [18] in conjugation with analytic gradient techniques.

The carbon, hydrogen and phosphor elements were described by Dunning-Huzinaga double-ζ (DZ) basis set [19, 20]. The corresponding contraction for C and H is (9s, 5p)/[4s, 2p], (4s)/[2s], while the phosphorus (11s, 7p)/[6s, 4p] basis set was augmented by polarization (*d*) function [21]. For the metal atoms the Stuttgart relativistic, small-core ECP [22, 23] basis set was used with cores of 10,28 and $60e^-$ for the first, second and third row respectively, whereas the valence electrons were described by (8s, 7p, 6d)/[6s, 5p, 3d]-contracted basis set. The energy as well as other properties were reevaluated in subsequent single-point calculations using the B3LYP functional [24] and somewhat extended basis sets. The carbon basis was extended with single sets of diffuse *sp* functions and a set of polarization (*d*) functions [19, 20]. A set of diffuse *p* functions was added to phosphorus, with the orbital exponent chosen to form a geometric series with the two most diffuse functions already present in the primitive basis set. Bond dissociation energies (BDE) for M–C_{60} were calculated from the energies of equilibrium structures of the complexes and their constituent fragments according to: $\mathrm{BDE(M-C_{60})} = \mathrm{E(C_{60})} + \mathrm{E(M)} - \mathrm{E(MC_{60})}$. Basis set superposition errors (BSSE) were estimated by the counterpoise correction method [25].

2.1.1.1 Atomic States

While calculation of atomic energies of closed-shell atoms is usually unproblematic, treatment of open-shell atoms with high multiplicity is often complicated when DFT is invoked. Contemporary DFT implementations rely on a single-determinant description of the non-interacting reference system, which implies that one can not apply linear combinations of determinants in order to describe a multiplet system correctly [26]. The course to take is to select a single-determinant non-interacting Kohn-Sham reference system that defines the proper values of the conserved quantum numbers. For the present metal system, the problem reduces to selecting the occupation of real, cartesian *nd*-orbitals that corresponds to a single determinant representation of the desired atomic term with correct angular momentum and spin symmetry. This has been addressed in Refs. [26, 27], and the guideline is to accept only solutions with the correct configuration within integer *d*-orbital occupations. To fulfill this requirement one frequently needs to make use of symmetry restrictions

given by non-Abelian point groups. For instance, octahedral symmetry with inversion (O_h) prevents *s*/*d* mixing since these orbitals belong to the different irreducible representations. In most difficult cases it is helpful to use of atomic orbitals obtained from restricted open-shell procedures as initial guesses for unrestricted calculation. Finally one should carefully check that the initially defined orbital assignment of electrons persists until convergence of the self-consistent field. Hay has made a convenient summary of proper occupations for some important *d*-states [27]. Occupations for the d^7, d^8 and d^9 states that are relevant to our systems are the following:

$(d^7s^2)^4F\ (d_{z^2})^2(d_{x^2-y^2})^2(d_{xy})^1(d_{xz})^1(d_{yz})^1$–Co, Ir
$(d^8s^1)^4F\ (d_{z^2})^1(d_{x^2-y^2})^1(d_{xy})^2(d_{xz})^2(d_{yz})^2$–Rh
$(d^9s^1)^3D\ (d_{z^2})^1(d_{x^2-y^2})^2(d_{xy})^2(d_{xz})^2(d_{yz})^2$–Ni,Pt.

It should be noted that for the nickel atom the ground state is often stated to be the ^3F term. Experimentally, the splitting between the ^3F and ^3D states is only 0.03 eV, with $(d^9s^1)^3D$ being the lower one [28].

2.1.1.2 Bonding Analysis

Atomic charges and orbital populations has been computed by means of Natural Bond Orbital analysis [29]. In order to estimate quantitatively the importance of ligand $\longrightarrow$ metal σ-donation and metal $\longrightarrow$ ligand π-back-donation to interaction energies, we used the Charge Decomposition Analysis (CDA) [30] method of Frenking and coworkers [30] as implemented in the AOMIX program [31, 32].

In this method the wave function of any given AB complex is expressed as a linear combination of the canonical molecular orbitals (Φ_μ) of the fragments A and B. The orbital contribution of the fragments to the wave functions of the complex accordingly to CDA method consists of the following terms

- charge donation σ from fragment A to fragment B (mixing of the occupied MOs of A fragment and the vacant MOs of fragment B):

$$\sigma_i = \sum_k^{occ,A} \sum_n^{vac,B} m_i c_{ki} c_{ni} \langle \Phi_k | \Phi_n \rangle \tag{2.1}$$

  where m_i is the occupation number of ith molecular orbital of AB complex, the summation of σ_i overall molecular orbitals gives the total charge donation (σ);
- back-donation π (mixing of the occupied MOs of B fragment and the vacant MOs of fragment A):

$$\pi_i = \sum_l^{occ,B} \sum_m^{vac,A} m_i c_{li} c_{mi} \langle \Phi_l | \Phi_m \rangle \tag{2.2}$$

- repulsive polarization r (closed-shell interaction of the occupied MOs of fragment A and B):

$$r_i = \sum_{k}^{occ,A} \sum_{m}^{occ,B} m_i c_{ki} c_{mi} \langle \Phi_k | \Phi_m \rangle \tag{2.3}$$

and the rest term Δ (mixing of vacant MOs) which can be used as indicator of bond covalency rather than a donor-acceptor nature of bond if $\Delta \gg 0$. The former term, repulsion has the negative sign and describes the amount of electronic charge removed from overlap of the occupied orbitals of the fragments into the nonoverlapping regions [30].

2.1.2 Results

2.1.2.1 Geometrical Parameters

The C_{60} Buckminsterfullerene has only two symmetry-unique bonds, corresponding to the junction of two six-membered rings (6–6′) and a six- and a five-membered ring (6–5). We have optimized the geometry of C_{60} under constraints of I_h symmetry, to obtain carbon–carbon bond lengths of 1.411 and 1.465 Å for the two unique distances. These values are in good agreement with data from electron diffraction studies [33], which gave values of 1.401 and 1.458 Å for these bond lengths. The curvature of this fullerene molecule may be characterized by the pyramidalization angle (δ), i.e. the angle between the projection of a specific C–C bond and a plane containing one of the designated carbons and its two adjacent atoms, cf Fig. 2.1. In our optimized C_{60} structure, the pyramidalization angle is in full agreement with the experimental value of 31°.

In order to validate the OLYP functional for the present use, we optimized C_{60}, as well as $Pd(PH_3)_2$- and $Pt(PH_3)_2$-C_{60} using first OLYP and then the B3LYP energy functional. Switching from OLYP to B3LYP induces only very minor changes in the bond distances of C_{60} (1.404 and 1.464 Å). For the metallofullerenes, optimized geometrical parameters are listed together with relevant experimental data in the Table 2.1. The two DFT methods leads to very similar results for the metal–carbon and carbon–carbon distances, whereas the metal–phosphorus distance systematically comes out longer at the B3LYP level of theory, by some 0.03 Å. From Table 2.1, there are significant differences between our geometry parameters and those obtained using the BP86 functional in Ref. [34]. Moreover, similar discrepancies are found between results obtained with OLYP and BP86 functionals for the corresponding ethylene complexes, cf the lower half of Table 2.1. This suggests that the difference is due to the choice of energy functional, since the two sets of BP86 results were obtained using different basis sets. In order to decide which is the better functional to use for this kind of study, it is desirable to make comparison to experimental structures. However, experimentally the triphenylphosphine ligand is used rather than phosphine itself, which complicates a direct comparison between theory and experiment. A comparison is further complicated by packing effects on the experimental X-ray

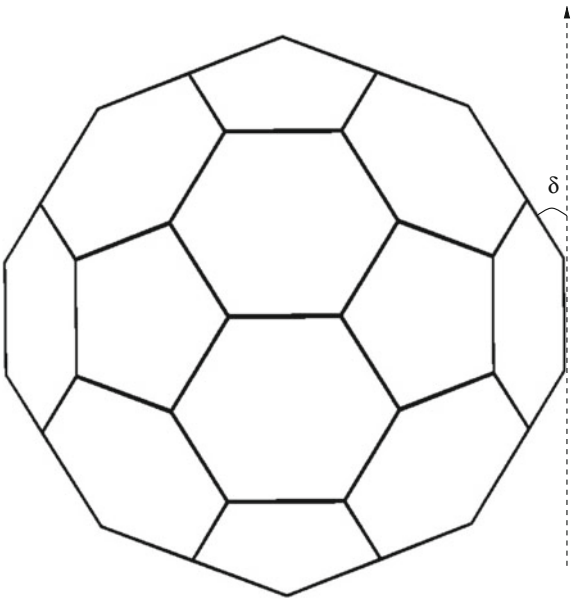

Fig. 2.1 Schematic representation of C_{60} and pyramidalization angle δ

structures, indicated by presence of inequivalent complexes in the unit cell, as well as distortion due to inclusion of solvent molecules in the crystal. The data included in Table 2.1 does not give a decisive edge to any of the functionals BP86 and OLYP, but rather serves to illustrate the level of uncertainty attached to both the experimental and theoretical structures.

Upon η^2-coordination of $M(PH_3)_2$ to a (6–6′) junction at C_{60}, interacting C–C bond extends to 1.489 Å in $Pd(PH_3)_2\eta^2$-C_{60} and to 1.516 Å in $Pt(PH_3)_2\eta^2$-C_{60}, quoting numbers obtained from OLYP. In the calculations, platinum approaches closer to the fullerene than does palladium, cf M–C distances of 2.14 and 2.16 Å, although the opposite is reported for the X-ray structure of the analogous triphenylphosphine complexes. The error bars are quite large, however, and prevents from drawing firm conclusions on this aspect.

2.1.2.2 Accuracy of OLYP

Let us consider accuracy of OLYP functional on the example of $Pt(PH_3)_2\eta^2$-C_{60}. This complex has been studied by different functionals such as B3LYP [35], BP86 [34, 36]. OLYP functional gives the best value for P–Pt–P angle (103.1°) versus BP86 [34] (107.4°) which is in a good agreement with the experiment [7] (102.4°). B3LYP value for P–Pt–P angle is in intermediate position (104.1°) between OLYP and BP86. The metal–phosphorus bond length has the same accuracy (2.297 Å) in OLYP and BP86 [36] calculations and quite close to the averaged experimental [7]

Table 2.1 Geometrical parameters as optimized for $M(PH_3)_2(\eta^2\text{-}C_{60})$ and $M(PH_3)_2(\eta^2\text{-}C_2H_4)$, M = Pd and Pt, and compared experimental data for the corresponding triphenylphosphine complexes

	rM–C	rC–C	rM–P	∠CMC	∠PMP	δ[a]
$Pd(PH_3)_2(\eta^2\text{-}C_{60})$						
OLYP	2.163	1.489	2.336	40.3	105.3	39.5
B3LYP	2.162	1.482	2.364	40.1	106.9	39.6
BP86[b]	2.180	1.464	2.378	39.2	111.0	38.8
$Pd(PPh_3)_2(\eta^2\text{-}C_{60})$ Exp[c]	2.123 [14]	1.447 [25]	2.330 [6]	40.2	109.7	40 [2]
	2.086 [16]		2.315 [5]			38 [2]
$Pt(PH_3)_2(\eta^2\text{-}C_{60})$						
OLYP	2.143	1.516	2.297	41.4	103.1	41.9
B3LYP	2.147	1.511	2.324	41.2	104.1	41.5
BP86[a]	2.103	1.505	2.289	41.9	107.4	41.8
$Pt(PPh_3)_2(\eta^2\text{-}C_{60})Exp$[d]	2.145 [24]	1.502 [30]	2.253 [7]	41.3 [8]	102.4 [2]	38 [2]
	2.115 [23]		2.303 [7]			44 [2]
$Pd(PH_3)_2(\eta^2\text{-}C_2H_4)$ OLYP	2.182	1.424	2.319	38.1	107.2	(19.3)
$Pd(PH_3)_2(\eta^2\text{-}C_2H_4)$ BP86[e]	2.195	1.401	2.312	37.2	112.5	–
$Pt(PH_3)_2(\eta^2\text{-}C_2H_4)$ OLYP	2.147	1.453	2.291	39.6	104.4	(24.5)
$Pt(PH_3)_2(\eta^2\text{-}C_2H_4)$ BP86[e]	2.152	1.431	2.286	39.0	108.7	–
$Pt(PPh_3)_2(\eta^2\text{-}C_2H_4)$ Exp[f]	2.106 [4]	1.434 [2]	2.270 [4]	39.7 [4]	111.60	
	2.116 [9]		2.265 [4]			

Bond lengths in Å, angles in degrees

[a]Pyramidalization angle as defined in the text. The definition is modified as angle between C–C projection and CH_2 plane when applied to the ethylene complexes

[b]Ref. [34]

[c]Ref. [9]

[d]Ref. [7]

[e]Ref. [52]

[f]Ref. [53]

value 2.278 Å. The calculated B3LYP value (2.324 Å) for Pt–P bond stands up far from the OLYP and BP86 results. The B3LYP Pt–P bond length (2.418 Å) reported in Ref. [35] overestimates the metal–phosphorus bond length. The fact is the Pt–P bond is very sensitive to the chosen basis set on phosphorus. We found out that inclusion of polarization function on phosphorus improves the value for Pt–P bond length significantly. The calculated BP86 [34] value 1.505 Å for interacting C–C distance agrees well with the experiment [7] 1.502 Å. The other BP86 [36] value 1.495 Å is also close to the experiment data. The corresponding bond distance obtained by OLYP functional 1.516 Å is somewhat longer. As one can see there is no unambiguous solution in the choice of functional. Each of the discussed functionals has the tendency to overestimate one parameter and underestimate the other. The results from OLYP geometry optimisation display good agreement with the experiment and comparable to accuracy of BP86 and B3LYP functional calculations.

2.1.2.3 Pd versus Pt in the Phosphine Complexes

It is noteworthy that Pd–C bond length in ethylene and fullerene complexes is longer than the Pt–C distance. This trend has been also observed at BP86 [34] level of theory. Kameno and coworkers [35] provide explanation to this trend which is based on the fact that the binding energy of $Pd(PH_3)_2$–C_{60} is smaller than that of Pt analogue. Indeed, we found similar consistency between the bond dissociation energy and metal–carbon distance in Pt and Pd compounds. However this can not be applied for Ni and Co analogues where the metal–carbon bond is shortest while the binding energy is lowest, but this will be the subject of our discussion below.

Also it is known that the inclusion of relativistic effects on heavy atoms shortens the metal–ligand bond distance in π-complexes significantly [37]. This being the case, the relativistic contraction equalizes Pt–C and Pd–C bond distances in $M(PH_3)_2C_2H_4$ complexes whereas nonrelativistic order gives Pd–C > Pt–C.

2.1.2.4 Ethylene versus C_{60}

The coordination of metal–phosphine ligand to ethylene results in deviation from planar structure. Calculated angular deformation between the C–C bond and CH_2 plane is 19.3° for $Pd(PH_3)_2C_2H_4$ and 24.5° for Pt analogue. Likewise the metal–ethylene bonding, in the case of fullerene the pyramidalization angle is increased upon coordination to metal atom from 31.7° in free C_{60} to 39.5° and 41.9° in Pd, Pt-fullerene derivatives (look Table 2.1). This effect is remarkable on the carbons at the reaction site. However at non-interacting region of C_{60} framework no significant perturbations in geometry have been found. Therefore exohedral interaction of metal atom with fullerene molecule is local phenomena.

In general, the geometry of $M(PH_3)_2(\eta^2C_{60})$ resembles precursor ethylene parent adduct $M(PH_3)_2(\eta^2$-$C_2H_4)$ except the fact that in fullerene complexes M–P and C–C bonds as a rule are slightly longer than in ethylene compounds (Table 2.1). Moreover the phosphorus in phosphine complexes prefer to stay in the same plane with the metal atom and interacting carbons of ethylene or fullerene molecule.

2.1.2.5 Binding Sites

We investigated the relative stability of fullerene complexes with different locations of palladium atom. For this purpose we optimised PdC_{60} structures with different hapticity, where metal atom is bound over pentagonal (η^5), hexagonal(η^6) rings and above two carbon atoms(η^2) of (6–6′) and (6–5) ring junction look Fig. 2.2. The cohesive energies corresponding to formation of palladium–fullerene bond are tabulated in Table 2.2. The most stable structure was found η^2 complex of metallofullerene in which palladium binds to carbons at the fusion of two six-membered rings (6–6′). This is in accord with the experiment since it is well-established that (6–6′) bonds of C_{60} is shorter than the (6–5) bonds and have the most double-bond character [38–40].

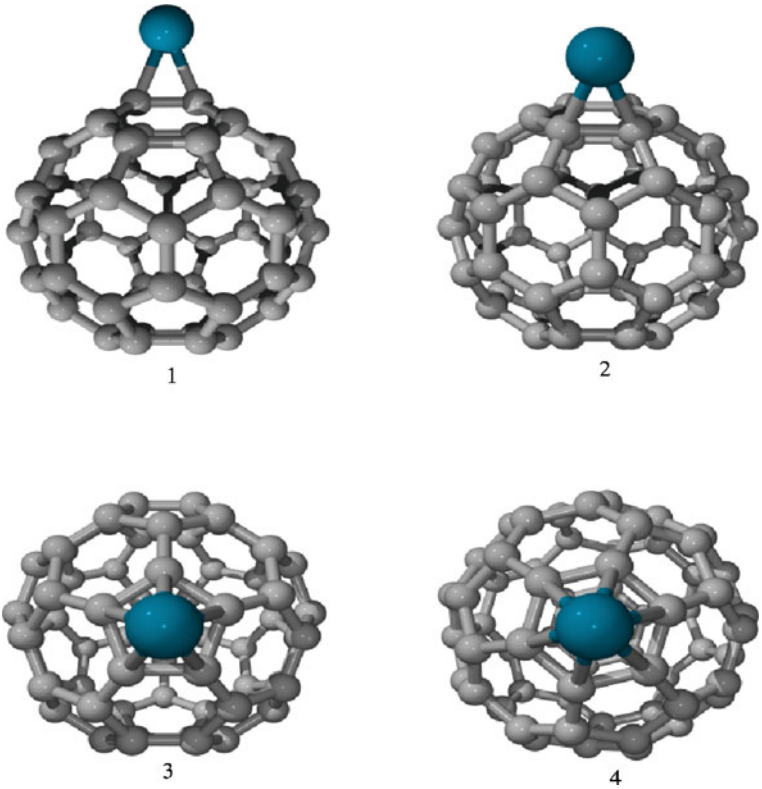

Fig. 2.2 Optimised structures of PdC_{60}: *1* η^2(6–6), *2* η^2(5–6), *3* η^5, *4* η^6

Table 2.2 Palladium bond dissociation energies (BDE) at different sites of C_{60} compound (kcal/mol), look Fig. 2.2

	η^2(6–6)	η^2(5–6)	η^5	η^6
BDE[a]	33.9	27.3	15.4	10.2
BSSE	1.9	1.9	2.8	2.5

[a]BSSE is not included

After we determined the most stable structure for PdC_{60} complex we expanded our investigations on stability of metallofullerenes for transition metals of group 9 and 10. Metal–fullrene bond dissociation energies, metal–carbon distances and pyramidalized angle are presented in Table 2.3. The coordination energies of naked metal atoms to C_{60} is found to increase down the groups, with the highest bond dissociation energy calculated for Pt–η^2C_{60}. Complexation of metal atom to C_{60} bond results in elongated C–C bonds at the site of metal coordination compared to those in C_{60} (Tables 2.1, 2.3). The electron-rich metal substance lowers the electron affinity of C_{60} by increasing electron population. Thus the resulting negative charge

Table 2.3 The bond dissociation energies (M–C_{60}) (kcal/mol), metal–carbon, carbon-carbon distances(Å) and pyramidalization angle of MC_{60}

M	Molecular state	BDE[a]	BSSE	R^{M-C}	$R^{C=C}$	δ
Co	$^2A_1$	7.7 (5.2)	2.6	1.951	1.514	40.4
Rh	$^2A_1$	37.9 (33.3)	1.9	2.073	1.510	40.1
Ir	$^2A_1$	41.7 (44.8)	2.1	2.054	1.531	41.3
Ni	$^1A_1$	23.3 (18.6)	2.5	1.912	1.508	39.8
Pd	$^1A_1$	33.9 (32.3)	1.9	2.114	1.485	38.2
Pt	$^1A_1$	49.7 (52.3)	2.0	2.060	1.516	40.0

[a]BSSE is not included; the bond dissociation energy of M–C_2H_4 is in parenthesis

Table 2.4 NBO charges of metal and interacting carbons, dipole moment (Debye) and HOMO-LUMO(ΔE) energy gap (eV) in the M–C_{60} complexes

Charge, e	Ni	Pd	Pt	Co	Rh	Ir
Metal	0.46	0.30	0.20	0.62	0.37	0.26
Carbon	−0.10	−0.050	−0.01	−0.15	−0.06	−0.02
μ	4.46	3.14	2.01	6.10	4.39	3.04
ΔE	2.34	2.48	2.49	1.96	2.43	2.44

Table 2.5 Bond dissociation energies BDE (kcal/mol) and dipole moment μ (Debye)

	BDE[a]	BSSE	μ		BDE[a]	BSSE	μ
Pt–C2H4	52.25	0.46	0.09	Pd–C2H4	32.27	0.40	0.60
Pt(PH3)2–C2H4	13.95	1.37	2.33	Pd(PH3)2–C2H4	11.55	1.16	1.87
$Pt(PH_3)_2$–C_{60}	17.83	4.81	9.17	$Pd(PH_3)_2$–C_{60}	16.55	4.32	8.05

[a]BSSE is not included

is mainly confined to the carbon atoms directly engaged in the interaction with the metal. In line with this, the dipole moments are moderate in magnitude despite the large size of these complexes, decreasing in groups from 4.5 D in NiC_{60} to 2.0 D in PtC_{60} and from 6.1 D in CoC_{60} to 3.0 D in IrC_{60} (Table 2.4). Addition of phosphine ligands to the metal atom increases the dipole moment significantly, but decreases metal–fullerene BDE look Table 2.5.

2.1.3 Discussion

It has been shown [41, 42] that partial donation of the π-electrons from alkene to an empty σ-orbital of the metal weakens the π-bond of the unsaturated hydrocarbon and therefore lowers π^* energy, which makes electrons easier accepted from a back-donating d-orbital of the metal atom. Transfer of electrons from the metal d-orbital to the antibonding π^* orbital increases the energy of the latter. As the consequence the degree of forming of metal–alkene bond should be reflected in HOMO-LUMO

energy gap of the complex. According to this mechanism the most strong M–C_{60} bond should have the metallofullerene complex with the largest HOMO-LUMO gap. In the complexes with various metal atoms the amount of charge transfer from fullerene to the metal as well as back-donation from metal to fullerene will be depend on the metal's *n*s and *n*d orbital energy. The lower *n*s–*n*d energy gap the better sd hybridisation and the stronger metal–fullerene bond is formed. The similar radial distribution of s and d orbitals facilitates sd hybridisation and therefore favors the interaction with the corresponding carbon orbitals.

Indeed inspection of the HOMO-LUMO(ΔE) gap in M–C_{60} complexes revealed correlation with the bond dissociation energy (BDE). The smallest energy gaps 1.96 and 2.34 eV were found for the top of group 9 and 10, namely Co,Ni, which are the most weakly bound to the fullerene (Table 2.4). Meanwhile the most stable compounds are Ir and Pt complexes. They have the largest HOMO-LUMO gap and the largest BDE in the groups. In fact the second- and third-row metals usually have stronger metal–carbon bonds than the first-row metals [43, 44]. The 5s and 4d orbitals of the second row metals contract much better than the 4s and 3d orbitals of the first-row metals.

Likewise, energy gap between s and d orbitals for second and third-row metal atoms is effectively smaller than for the first-row metal atoms [45]. The strength of the metal–alkene bond depends on the degree of spatial overlap of atomic orbitals which occur during approaching of metal atom to the alkene. In order to achieve the proper overlap the sd/sp hybridisation should occur in metal atom. The hybridisation relieves the repulsion between the ns orbital of metal atom and π orbital of alkene due to the fact that one of the hybrid orbital accumulates the electronic charge in nonbonding region [46]. At the same time the other hybrid orbital becomes the acceptor orbital, which is oriented along the coordination plane.

We used radius and energy values of s, d orbitals as variables for prediction of BDE (look Fig. 2.3). The correlation coefficient (r) is equal to 0.91 and defined as:

$$r = \frac{C_{ij}}{\sqrt{C_{ii}C_{jj}}} \tag{2.4}$$

where C_{ij} is covariance between calculated and predicted data sets and C_{ii}, C_{jj} are standard deviations.

The BDEs based on this model is in qualitative agreement with calculated BDEs however it overestimates energy values for Co and underestimates for Ni i.e. it deviates in the cases where promotion energy should be taken into account.

From the Table 2.4 one can notice that Co has the lowest BDE. This is also supported by experiment since the neutral Co atom show no reaction neither with ethene [47] nor with fullerene [13].

The low bond dissociation energy of cobalt–fullerene(ethene) compounds can be explained in terms of s–d hybridisation mentioned above, loss of exchange and promotion energies. For the beginning it should be noted that atomic ground state of neutral cobalt is $3d^7 4s^2$. According to ab initio calculations [48, 49] $M(d^{n-2}s^2)$ +

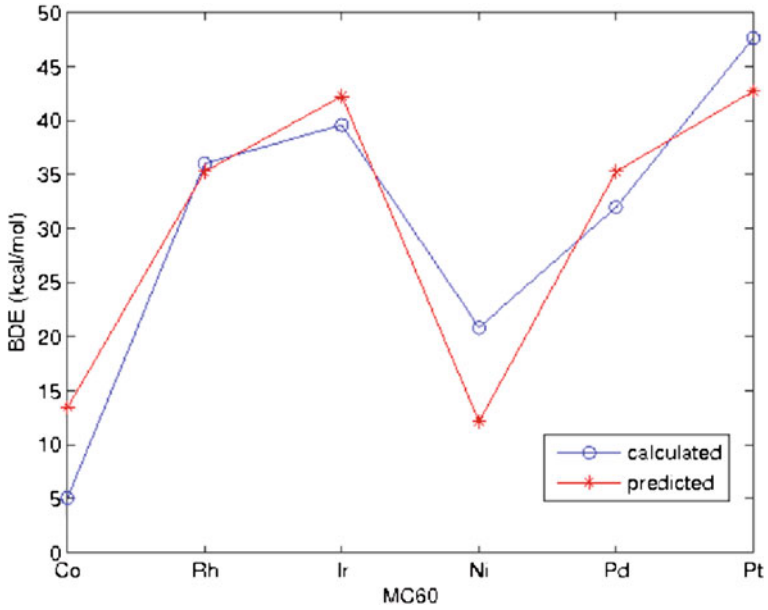

Fig. 2.3 Linear regression model for BDE of MC_{60}. *Blue line* is calculated BDEs; *red line* is predicted BDE based on radii extension and energy gap of s, d orbitals

C_2H_4 asymptotes exhibit only repulsive potentials. Essential metal–alkene binding arises only from attractive $d^{n-1}s$ asymptotes. In order to reach excited $d^{n-1}s$ state cobalt atom should obtain promotion energy at least 10 kcal/mol [28]. Our own calculations determine 13 kcal/mol promotion energy to $d^{n-1}s$ state of low-spin for the cobalt and only 3 kcal/mol for the nickel atom. Only in such bond prepared state the metal atom can hybridise and form the bond with the alkene. Contribution to low BDE of Co atom gives also large s/d energy gap and large ratio between radii extension of these orbitals. For the other complexes with the strong metal–fullerene bond these parameters have significantly smaller values.

Considering M–C_{60} interaction in terms of Dewar–Chatt–Duncanson model [50, 51] one should study in a couples σ-donation of π-electrons to the metal and a π-bond back-donation from metal to the lowest vacant orbitals of interacting carbon (6–6′) bond.

Table 2.6 summarizes total donation, back-donation and repulsion terms for metallofullerenes and for the M–C_2H_4 parent adduct. Both ethylene and fullerene complexes have common peculiarities: σ donation decreases downwards the group, while π back-donation has the opposite trend and increases in the group with the increasing of nuclear charge of the metal. For the late transition metals studied here, except of the first-row transition metals (Co, Ni), the metal–C_{60}/C_2H_4 bond is dominated by back-donation. We found that the M–C_{60}/C_2H_4 bond strength correlates with the donation and back-donation (look Tables 2.3, 2.6). BDE increases with the

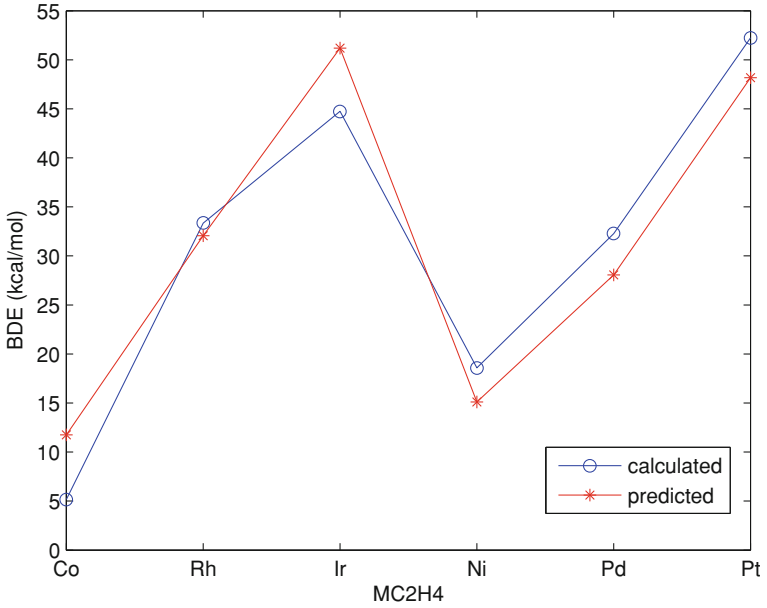

Fig. 2.4 Linear regression model for BDE of MC_2H_4. *Blue line* is calculated BDEs; *red line* is predicted BDE based on π, σ variables

increasing of π back-donation and decreasing of σ donation. For example the largest values for back-donation 0.42 e exhibits the Ir and Pt-fullerene complexes, which have also the largest BDE 42 and 50 kcal/mol respectively. We used multivariate method of analysis for processing of BDE, σ and π data. The correlation diagrams are presented in Fig. 2.4 for MC_2H_4 and in Fig. 2.5 for MC_{60}. Obtained correlation coefficient of regression model based on two variables, σ and π is 0.99 for PdC_{60}. The corresponding correlation coefficient for PdC_2H_4 is 0.95.

This type of behavior in BDE and charge transfer between fullerene and metal atoms can be understood on the ground of the s and d orbital energies of the metal atom. As we mentioned above the size and energy of s, d orbitals play an important role in the metal–fullerene bonding. It is clear that if the energy of d orbital rises then the back donation will increase too, and with the lowering of s orbital energy one can expect decreasing of σ donation. Since down the group the d orbital energy increases the same trends one can observe in back-donation process, which leads to the corresponding trend in BDE. And the results from the Tables 2.3, 2.6 supports this conclusion. Inspection of the repulsion term shows significant closed-shell repulsion for the Rh and Pd species. The reduced repulsive polarization in metallofullerene complexes in comparison to the metal–ethylene compounds is assumed due to the reduction of electron occupancy on interacting carbon (6–6′) bond of fullerene molecule. The NBO population of this bond in pure fullerene is 1.64 whereas in ethylene

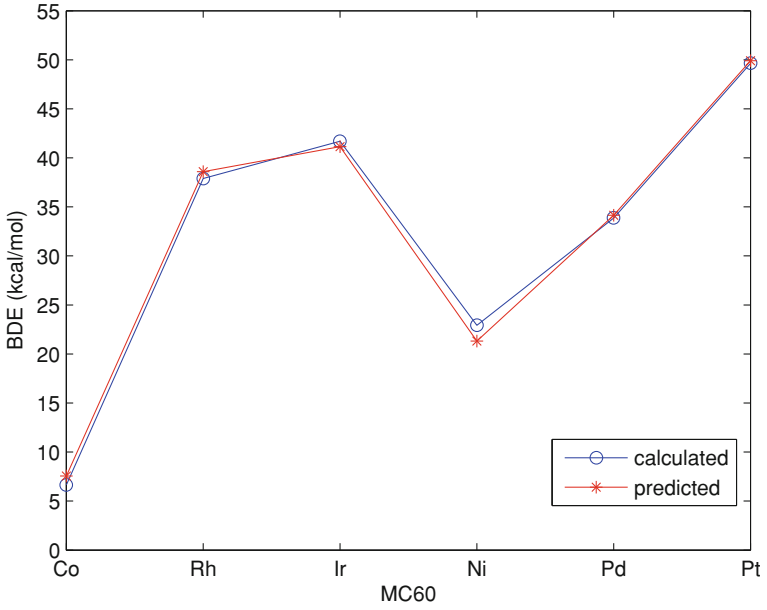

Fig. 2.5 Linear regression model for BDE of MC_{60}. *Blue line* is calculated BDEs; *red line* is predicted BDE based on π, σ variables

Table 2.6 Charge decomposition analysis of MC_{60}[a] and MC_2H_4: donation (σ), back-donation (π) and repulsion (r)

MC_{60}	σ	π	r	MC_2H_4	σ	π	r
CoC_{60}	0.33	0.20	−0.11	CoC_2H_4	0.42	0.22	−0.21
RhC_{60}	0.22	0.37	−40.20	RhC_2H_4	0.20	0.32	−0.34
IrC_{60}	0.12	0.42	−0.17	IrC_2H_4	0.08	0.41	−0.14
NiC_{60}	0.32	0.26	−0.10	NiC_2H_4	0.31	0.24	−0.02
PdC_{60}	0.25	0.34	−0.18	PdC_2H_4	0.25	0.30	−0.35
PtC_{60}	0.21	0.42	−0.15	PtC_2H_4	0.22	0.39	−0.24

[a]CDA based on DZP basis set calculations (In order to fulfil the requirement of AOMIX program 'Number of canonical orbitals = number of basis functions' and to avoid linear dependency problem we had to run B3LYP single point calculations without diffuse basis function on carbon. Obtained BDE are very much similar to the previous and does not differ from them by more than 0.3 kcal/mol)

molecule the population of C–C bond is close to the double occupancy. Thus the repulsive polarization in MC_{60} is less than metal–ethylene four electron repulsion.

It should be noted that the difference between the amount of donation and back-donation is not equal to the charge transfer between metal and fullerene. This is because the terms donation and back-donation according to CDA method [30] do not include only charge transfer interactions but rather describe an overall reorganization of electronic density. The stronger electronic polarization the greater deviation

between the difference of donation and back-donation and the net charge transfer is expected [31, 32].

2.1.4 Conclusions

The different types of structures on the ground state of selected MC_{60}, have in the present work been discussed together with the interpretation of bond dissociation energies. In general the site above a 6–6′ ring junction leads to an attractive interaction.

Two DFT methods, namely OLYP and B3LYP, have been compared via geometrical parameters and stability of various exohedral metallofullerene structures.

The M–C_{60} bonds are analyzed in terms of Charge Decomposition Analysis giving quantitative estimates of electron donation, back donation and repulsive polarization. The π back-donation has the dominant contribution to the metal–fullerene bond for the second and third row metal–fullerene bond for the second and third row metal MC_{60}/C_2H_4 complexes. We found and interpreted the correlation between BDE and amount of π back-donation and σ donation.

The weak Co–C_{60} bond is due to the large promotion energy of neutral cobalt atom to the excited bond-prepared state.

The charge decomposition analysis based on linear combination of fragment molecular orbitals is proved to be very useful tool for studying interaction between molecular fragments in terms of donation, back-donation and polarization.

2.2 Multiple Doping

2.2.1 Overview

A number of compounds in which fullerene cages are exohedrally and multiply doped with bare alkali [54], alkaline earth [54] or transition metal atoms [54–59] have been synthesized and isolated. Examples of the latter include M_nC_{60}, M = Ti, Nb, Re, Fe, Ru, Ni, Pd and Pt. For M_nC_{60} n > 1 only Ni_nC_{60} has been investigated theoretically [60, 61]. Most of the experimental attention has been directed toward palladium-and platinum-doped C_{60} [54, 56, 59, 62], and by varying the reaction conditions, Pd_nC_{60} with $n = 1 - 7$ may be synthesized [63]. Difficulties in obtaining single crystals of the required size and quality [54] have meant that only limited structural information is available for these compounds. The monosubstituted fullerene PdC_{60} is believed to exist as a linear polymer, with palladium atoms alternating with C_{60} units [55]. Structures with higher degree of doping, i.e. n > 1 are assumed to have crosslinks between monomer chains [55].

Palladium–fullerene complexes exhibit catalytic activity with respect to hydrogenation of unsaturated hydrocarbons [55, 63]. It has been suggested that there are two types of metal atoms in Pd_nC_{60}, and that palladium atoms bridging neighboring fullerene units are catalytically inactive [55, 63]. The palladium particles responsible for the catalytic activity are believed to be "excessive" metal atoms adsorbed on the surface of C_{60} [55, 63]. A clear picture of how multiple metal atoms arrange on the fullerene surface is, however, not available, and it is not known whether the "excessive" metal atoms adsorb individually or form metal clusters on the fullerene surface.

The aim of the present contribution is to identify the preferred structures of C_{60} with two or more bare palladium atoms adsorbed, as well as to assess the associated Pd-fullerene bond energies. To this end we use density functional theory to optimize the geometry of the molecules and to compute the binding energy of palladium atoms at different sites.

Formation of equivalent bonds in metal–ligand bonding is referred to as hapticity (η), and in the case of exohedral metallofullerenes, single atoms may in principle explore the range from one to six for η, depending on the site of coordination to the fullerene. To our knowledge, only η^2-substituted exohedral metallofullerenes have been observed so far and in the present work we focus on this coordination mode.

The study disregards interactions between fullerene cages, and as such pertains to a gas or dilute solution of these compounds, and to the solid phase only to the extent that metal atoms not taking part in fullerene bridging are taken into consideration.

2.2.2 Computational Details

Metallofullerene geometries were optimized using analytic gradient techniques and the OLYP density functional. For Pd, the Stuttgart relativistic $28e^-$ small core ECP [64] was used in conjunction with a (8s, 7p, 6d)/[6s, 5p, 3d]-contracted valence basis set. Properties were obtained in subsequent single-point energy evaluations using the B3LYP functional with a carbon atom basis set that was extended with diffuse and polarization functions compared to that applied in the geometry optimizations. Basis set superposition errors (BSSE) were estimated by the counterpoise correction method. Further details and references can be found in Ref. [65].

2.2.3 Results and Discussion

A single palladium atom binds preferentially in η^2-mode to the junction between two hexagons (6–6′)onC_{60}. In Fig. 2.7 we systematically add palladium atoms to C_{60} at sites that allow for this preferred binding mode while avoiding metal–metal interactions as far as possible. Complexation of a Pd atom induces elongation of the interacting carbon–carbon bond from 1.411 Å in pure C_{60} (the corresponding bond

Table 2.7 Bond dissociation energies (BSSE corrected) of $Pd_{n-1}(\eta^2\text{-}C_{60})$-Pd, n = 1–6

n	1	2	3	4	5	6
BDE (kcal/mol)	32.0	31.9	31.8	31.6	31.6	31.7

distance from electron diffraction is 1.401 Å [66]) to 1.482–1.485 Å in the metallofullerenes. Moreover, the atomic charge and orbital occupancy of the palladium atom first added is only weakly affected by the additional metal atoms. For instance, its NBO charge drops from 0.30*e* in the monosubstituted fullerene to 0.27*e* in Pd_6C_{60}.

The interaction between transition metal atoms (M) and fullerenes is often characterized in terms of the *Dewar–Chatt–Duncanson* model [67, 68], which implies electron donation from bonding orbitals at the organic ligand into unoccupied *d* orbitals of σ symmetry at the metal as well as back donation from metal *d*-orbitals of π symmetry into vacant π^*. Molecular orbitals at the interacting carbon–carbon double bond. We find that this picture describes the η^2-coordinated Pd atom well at a (6–6′) junction. The occupancy of the donating Pd d_π-orbital remains essentially constant at 1.64 *e* as additional metal atoms are adsorbed.

In line with the results from the population analysis, the bond dissociation energy (BDE) of each Pd atom remains almost constant, at 32 kcal/mol, for up to 6 added metal atoms (Table 2.7). Evidently, the binding of single metal atoms is a local phenomenon, and only small perturbations propagate through the delocalized π system to neighboring sites. Moreover, the fullerene appears to be a very soft ligand, meaning that its electron-accepting capacity is very slowly saturated, as long as the adsorbed metal atoms are evenly distributed. At this point it is interesting to explore whether the adsorbed Pd atoms have a tendency to cluster together at the surface, and, moreover, whether such a metal cluster would desorb from the fullerene once it is formed. We investigated the relative stability of different disubstituted exohedral metallofullerenes by optimizing structures (**1**–**5**, Fig. 2.7) with different locations of the second Pd atom relative to the palladium atom of PdC_{60} (cf. Fig. 2.6).

Structures **1** and **2** both correspond to η^2 coordination of the two metal atoms over the same hexagon. In **2** both Pd atoms coordinate to (6–6′) junctions. This ensures an optimal bond for each metal atom to the fullerene and at the same time allows for some metal–metal interaction; r(Pd − Pd) = 3.01 Å. In **1**, on the other hand, one of the metal atoms coordinates to a (6–5) junction, and the bond dissociation energy of the second palladium atom drops by more than 10 kcal/mol compared to that of **2**, see Table 2.8. The reason for this may be sought in the occupancy of the donating lone-pair orbital for Pd. For the Pd atom adsorbed above the (6–6′) junction in structure **1** the number of electrons in this orbital (NBO population) is 1.69 (Table 2.8), only to increase to 1.76 if we consider the metal atom coordinated to a (6–5) junction. Clearly, the most effective back donation is achieved when the metal coordinates to (6–6′) sites. Structure **3** resembles that of **2**, except that the two metal atoms are further removed from each other. The BDE is only 2 kcal/mol lower than that of **2**, indicating the magnitude of the metal–metal interaction in the latter. Structures **4** and

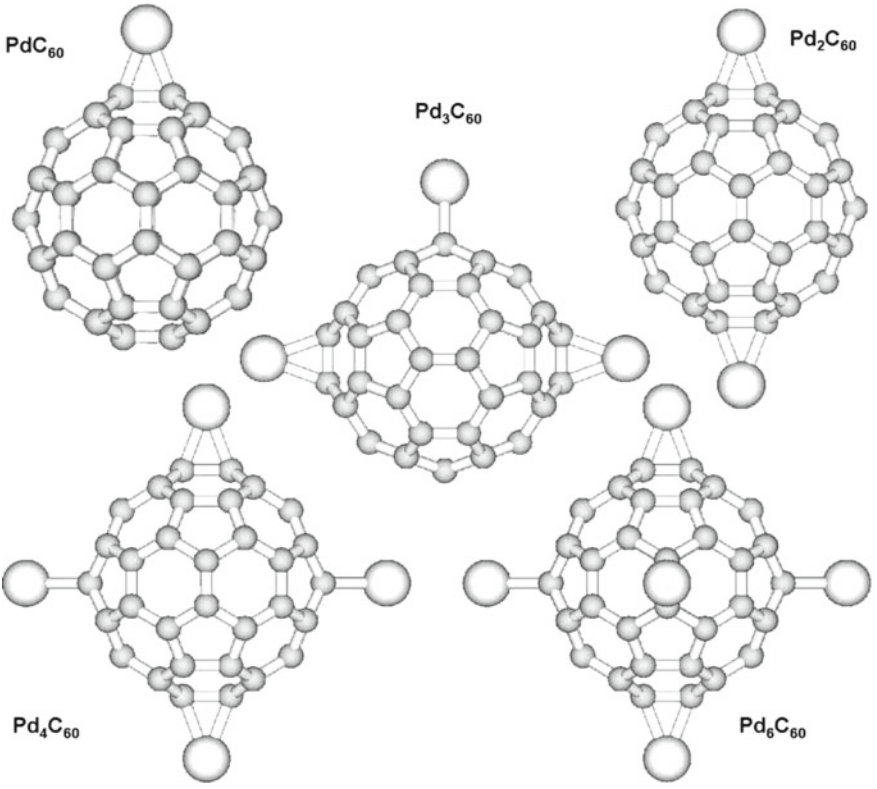

Fig. 2.6 Optimized exohedral metallofullerenes Pd_nC_{60} (n.1, 2, 3, 4, and 6)

Table 2.8 Bond dissociation energies (BDE) of PdC_{60}–Pd bonds and electronic properties of Pd_2C_{60}

Structure[a]	1	2	3	4	5
BDE[b](kcal/mol)	23.0(2.0)	34.6(1.9)	32.4(1.8)	10.0(0.5)	33.8(1.7)
Pd_1 $4d_\pi$ population[c]	1.69	1.75	1.63	1.61	1.69
Charge on Pd_1(e)[c]	0.29	0.26	0.29	0.17	0.22

5 describe coordination of a well-defined palladium dimer (Pd_2) in a singlet spin state, either end-on (**4**) or side-on (**5**), the latter structure featuring η^1 coordination mode to a (6–6′) junction of the fullerene molecule. The bond distances in the dimer are 2.76 and 2.63 Å in **4** and **5**, respectively. The end-on structure supports a very low BDE for the second palladium atom, reflecting that it binds to a less electronegative metal atom rather than directly to the fullerene. The two most stable structures found, (**2** and **5**), both maintain a Pd–Pd interaction while allowing both metal atoms to adsorb at (6–6′) junctions.

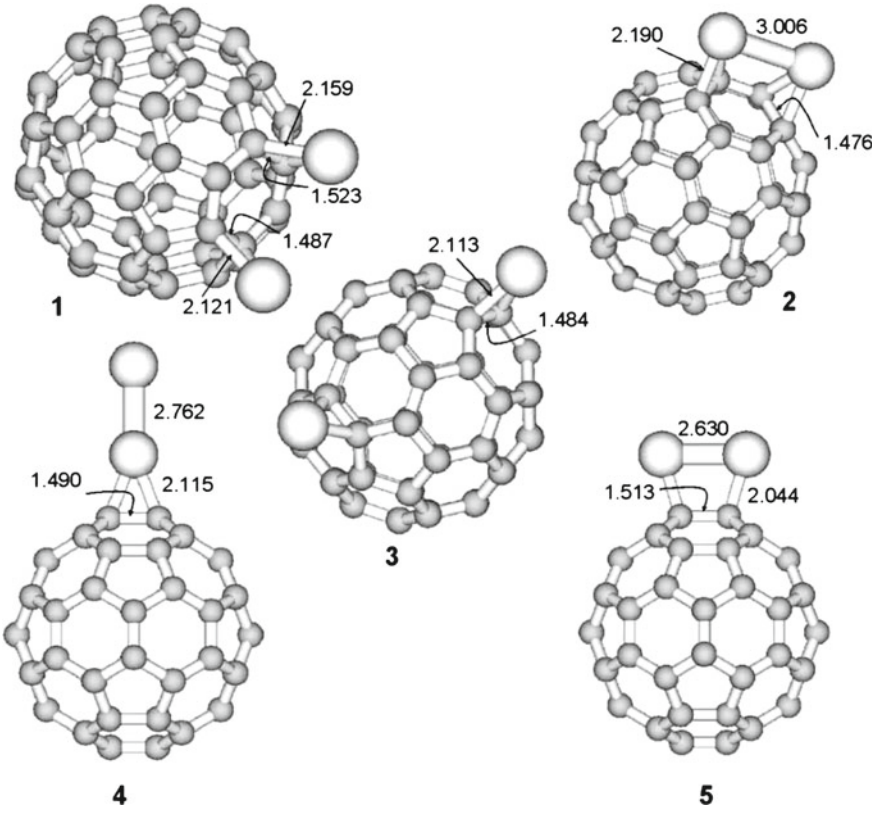

Fig. 2.7 Optimized exohedral metallofullerenes Pd_2C_{60}. *Curved* (*straight*) *arrows* point to C–C (C–Pd) bonds

For the Pd dimer, the ground state was identified as a triplet spin state, having an equilibrium bond length of 2.53 Å. The computed bond dissociation energy (20.5 kcal/mol) is in qualitative agreement with the experimental values (17 ± 4, 26 ± 5) [69]. Furthermore, it is much lower than twice the Pd-fullerene bond energy and clearly demonstrates that metal dimerization can not compete with metal adsorption onto the fullerene.

2.2.4 Conclusions

Density functional theory calculations show that the Pd–C_{60} bond energy remains essentially constant for up to six palladium atoms that are individually adsorbed onto C_{60}. A novel $Pd_2(\eta^2\text{-}C_{60})$ structure (**2** in Fig. 2.7) has been identified as the most stable arrangement of two palladium atoms on the external surface of C_{60}. It

shows the two metal atoms bridging over a single six-membered ring, with both atoms benefiting from η^2 coordination at (6–6′) junctions as well as some metal–metal interaction. However, the difference in enthalpy between **2** and competing structures without metal–metal interaction is only 2 kcal/mol. Entropy considerations suggest that both isolated atoms and weakly bonded metal aggregates may exist in equilibrium. Binding of Pd atoms to the fullerene is preferred over palladium dimerization.

References

1. Sulman, E., Matveeva, V., Semagina, N., Yanov, I., Bashilov, V., Sokolov, V.: J. Mol. Catal. **146**, 257 (1999)
2. Claridge, J., Douthwaite, R., Green, M.: J. Mol. Catal. **89**, 113 (1994)
3. Nagashima, H., Nakaoka, A., Tajima, S., Saito, Y., Itoh, K.: Chem. Lett. **7**, 1361 (1992)
4. Nagashima, H., Kato, Y., Yamaguchi, H., Kimura, E., Kawanishi, T., Kato, M.: Saito, Y., Haga, M., Itoh, K. Chem. Lett. **7**, 1207 (1994)
5. Wohlers, M., Herzog, B., Belz, T., Bauer, A., Braun, T., Ruhle, T., Schlogl, R.: Synth. Met. **77**, 55 (1996)
6. Braun, T., Wohlers, M., Belz, T., Nowitzke, G., Wormann, G., Uchida, Y.: Pfander, N., Schlogl, R. Catal. Lett. **43**, 167 (1997)
7. Fagan, P., Calabrese, J., Malone, B.: Science **252**, 1160 (1991)
8. Fagan, P., Calabrese, J., Malone, B.: Acc. Chem. Res. **25**, 134 (1992)
9. Bashilov, V., Petrovskii, P., Sokolov, V., Lindeman, S., Guzey, I., Struchkov, Y.: Organometallics **12**, 991 (1993)
10. Dresselhaus, M., Dresselhaus, G., Eklund, P.: Science of Fullerenes and Carbon Nanotubes. Academic press Inc., San Diego (1996)
11. Lerke, S.A., Evans, D.H., Fagan, P.J.: J. Am. Chem. Soc. **114**, 7807 (1992)
12. Fagan, P.J., Calabrese, J.C., Malone, B.: J. Am. Chem. Soc. **113**, 9408 (1991)
13. Talyzin, A.V., Jansson, U.: Thin Solid Films **429**, 96 (2003)
14. Fujimoto, H., Nakao, Y., Fukui, K.: J. Mol. Struct. **300**, 425 (1993)
15. Lichtenberger, D., Wright, L., Gruhn, N., Rempe, M.: J. Organomet. Chem. **478**, 213 (1994)
16. Andriotis, A., Menon, M.: Phys. Rev. **60**, 4521 (1999)
17. Alemany, M., Dieguez, O., Rey, C., Gallego, L.: J. Chem. Phys. **114**, 9371 (2001)
18. Handy, N., Cohen, A.: J. Mol. Phys. **99**, 403 (2001)
19. Dunning Jr, T.H.: J. Chem. Phys. **53**, 2823 (1970)
20. Dunning, T., Hay, P.: Methods of Electronic Structure Theory. In: Schaeffer, H. (ed.) Modern theoretical chemistry. Plenum Press, New York (1977)
21. Magnusson, E., Schaefer III, H.: J. Chem. Phys **83**, 5721 (1985)
22. Dolg, M., Wedig, U., Stoll, H., Preuss, H.: J. Chem. Phys. **86**, 866 (1987)
23. Andrae, D., Haeussermann, U., Dolg, M., Stoll, H.: Theor. Chim. Acta **77**, 123 (1990)
24. Becke, A.: J. Chem. Phys. **98**, 5648 (1993)
25. Boys, S., Bernardi, F.: Mol. Phys. **19**, 553 (1970)
26. Koch, W., Holthausen, M.: A Chemist's Guide to Density Functional Theory. Wiley-VCH, Weinheim (2000)
27. Hay, P.: J. Chem. Phys. **66**, 4377 (1977)
28. Moore, C.: Atomic Energy Levels. NBS, Washington (1958)
29. Glendening, E., Reed, A., Carpenter, J., Weinhold, F.: NBO Version 3.1. (2001)
30. Dapprich, S., Frenking, G.: J. Phys. Chem. **99**, 9352 (1995)
31. Gorelsky, S.I.: AOMix: Program for Molecular Orbital Analysis. York University, Toronto (1997). http://www.sg-chem.net/

32. Gorelsky, S., Lever, A.: J. Organomet. Chem **635**, 187 (2001)
33. Hedberg, K., Hedberg, L., Bethune, D., Brown, C., Dorn, H., Johnson, R., de Vries, M.: Science **254**, 410 (1991)
34. Nunzi, F., Sgamellotti, A., Re, N., Floriani, C.: Organometallics **19**, 1628 (2000)
35. Kameno, Y., Ikeda, A., Nakao, Y., Sato, H., Sakaki, S.: J. Phys. Chem. **109**, 8055 (2005)
36. Campanera, J., Munoz, J., Vazquez, J., Bo, C., Poblet, J.: Inorg. Chem. **43**, 6815 (2004)
37. Li, J., Schreckenbach, G., Ziegler, T.: Inorg. Chem. **34**, 3245 (1995)
38. Hawkins, J., Meyer, A., Lewis, T., Loren, S., Hollander, F.: Science **252**, 312 (1991)
39. Fagan, P., Ward, M., Calabrese, J.: J. Am. Chem. Soc. **111**, 1719 (1989)
40. Haser, M., Almlof, J., Scuseria, G.: Chem. Phys. Lett. **181**, 497 (1991)
41. Morokuma, K., Borden, W.: J. Am. Chem. Soc. **113**, 1912 (1991)
42. Blomberg, M., Siegbahn, P., Svensson, M.: J. Phys. Chem. **96**, 9794 (1992)
43. Gates, B.: Catalytic Chemistry. Wiley, New York (1992)
44. Blomberg, M., Siegbahn, P., Nagashima, U., Wennerberg, J.: J. Am. Chem. Soc. **113**, 424 (1991)
45. Visscher, L., Dyall, K.: Atomic Data Nucl. Data Tables **67**, 207 (1997)
46. Weisshaar, J.: ACS Symp. Ser. **530**, 208 (1993)
47. Ritter, D., Weisshaar, J.: J. Am. Chem. Soc. **112**, 6425 (1990)
48. Widmark, P., Roos, B., Siegbahn, P.: J. Phys. Chem. **89**, 2180 (1985)
49. Siegbahn, P., Brandemark, U.: Theor. Chim. Acta **69**, 119 (1986)
50. Chatt, J., Duncanson, L.: J. Chem. Soc. **1953**, 2939 (1953)
51. Dewar, M.: Bull. Soc. Chim. Fr. p. 71(1951)
52. Massera, C., Frenking, G.: Organometallics **22**, 2758 (2003)
53. Cheng, P., Nyburg, S.: Can. J. Chem. **50**, 912 (1972)
54. Dresselhaus, M.S., Dresselhaus, G., Eklund, P.C.: Science of Fullerenes and Carbon Nanotubes. Academic Press, San Diego (1996)
55. Nagashima, H., Nakaoka, A., Saito, Y., Kato, M., Kawanishi, T., Itoh, K.: The first organometallic polymer of buckminsterfullerene. J. Chem. Soc. Chem. Commun. **69**, 377–379 (1992)
56. Nagashima, H., Kato, Y., Yamaguchi, H., Kimura, E., Kawanishi, T., Kato, M.: Haga, M., Itoh, K.: Synthesis and reactions of organoplatinum compounds of C_{60}, $C_{60}Pt_n$. Chem. Lett. **7**, 1207–1210 (1994)
57. Ivanova, V.N.: Fullerene compounds with transition metals M_nC_{60}: preparation, structure, and properties. J. Struct. Chem. **41**, 135–148 (2000)
58. Wohlers, M., Herzog, B., Belz, T., Bauer, A., Braun, Th, Ruhle, Th, Schlogl, R.: Ruthenium-C_{60} compounds: Properties and catalytic potential. Synth. Met. **77**, 55–58 (1996)
59. Talyzin, A.V., Jansson, U.: A comparative Raman study of some transition metal fullerides. Thin Solid Films **429**, 96–101 (2003)
60. Alemany, M.M.G., Dieguez, O., Rey, C., Gallego, L.J.: A densityfunctional study of the structures and electronic properties of C_{59}Ni and C_{60}Ni clusters. J. Chem. Phys. **114**, 9371–9374 (2001)
61. Andriotis, A.N., Menon, M.: Geometry and bonding in small $(C_{60})_nNi_m$ clusters. Phys. Rev. B **60**, 4521–4524 (1999)
62. Nagashima, H., Yamaguchi, H., Kato, Y., Saito, Y., Haga, M., Itoh, K.: Facile cleavage of carbon-palladium bonds in $C_{60}Pd_n$ with phosphines and phosphites. An alternative route to $(\eta^2 - C_{60})PdL_2$ and discovery of fluxionarity suggesting the rotation of C_{60} on the PdL_2 species in solution. Chem. Lett. **12**, 2153–2156 (1993)
63. Nagashima, H., Nakaoka, A., Tajima, S., Saito, Y., Itoh, K.: Catalytic hydrogenation of olefins and acetylenes over $C_{60}Pd_n$. Chem. Lett. **377**, 1361–1364 (1992)
64. Andrae, D., Haeussermann, U., Dolg, M., Stoll, H., Preuss, H.: Energyadjusted ab initio pseudopotentials for the second and third row transition elements. Theor. Chim. Acta **77**, 123–141 (1990)
65. Sparta, M., Jensen, V.R., Borve, K.J.: Structure and stability of substitutional metallofullerenes of the first-row transition metals. Fuller. Nanotub. Carb. Nanostruct. **14**(2–3), 269–278 (2006)

66. Hedberg, K., Hedberg, L., Bethunde, D.S., Brown, C.A., Dorn, H.C., Johnson, R.D., Devries, M.: Bond lengths in free molecules of buckminsterfullerene, C_{60}, from gas-phase electron-diffraction. Science **254**, 410–412 (1991)
67. Chatt, J., Duncanson, L.A.: Olefin co-ordination compounds 3. Infrared spectra and structure-attempted preparation of acetylene complexes. J. Chem. Soc. **28**, 2939–2947 (1953)
68. Dewar, M.J.S.: A review of the π-complex theory. Bull. Soc. Chim. Fr. **18**, C71–79 (1951)
69. Lin, S.S., Strauss, B., Kant, A.: Dissociation energy of Pd_2. J. Chem. Phys. **51**, 2282–2283 (1969)

http://www.springer.com/978-3-642-31844-3

Quantum-chemical studies on Porphyrins, Fullerenes and Carbon Nanostructures

Loboda, O.

2013, XVIII, 154 p., Hardcover
ISBN: 978-3-642-31844-3